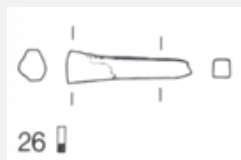


# TANG FRAGMENT OF A KNIFE HR-6567 - LEADED BRONZE - LATE BRONZE AGE - SWITZERLAND

<b>Artefact name</b>	Tang fragment of a knife HR-6567
<b>Authors</b>	Marianne. Senn (EMPA, Dübendorf, Zurich, Switzerland) & Christian. Degrigny (HE-Arc CR, Neuchâtel, Neuchâtel, Switzerland)
<b>Url</b>	/artefacts/381/

## ∨ The object



Credit HE-Arc CR.

Fig. 1: Leaded bronze tang fragment (after Rychner-Faraggi 1983, plate 35.26),

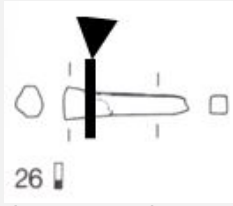
## ∨ Description and visual observation

<b>Description of the artefact</b>	Tang fragment with shiny brown patina typical of lake context (Fig.1). Dimensions: L = 2.9cm; Ømax. = 6.8mm; WT = 4.9g.
<b>Type of artefact</b>	Knife
<b>Origin</b>	Hauterive - Champréveyres, Neuchâtel, Neuchâtel, Switzerland
<b>Recovering date</b>	Excavation in 1983-1985, layer 3
<b>Chronology category</b>	Late Bronze Age
<b>chronology tpq</b>	<input type="text" value="1054"/> B.C. ∨
<b>chronology taq</b>	<input type="text" value="1000"/> B.C. ∨
<b>Chronology comment</b>	Hallstatt B1 (1054/1037BC_ 1000BC)
<b>Burial conditions / environment</b>	Lake
<b>Artefact location</b>	Laténium, Neuchâtel, Neuchâtel
<b>Owner</b>	Laténium, Neuchâtel, Neuchâtel
<b>Inv. number</b>	Hr 6567
<b>Recorded conservation data</b>	Not conserved

## Complementary information

Nothing to report.

Study area(s)



Credit HE-Arc CR.

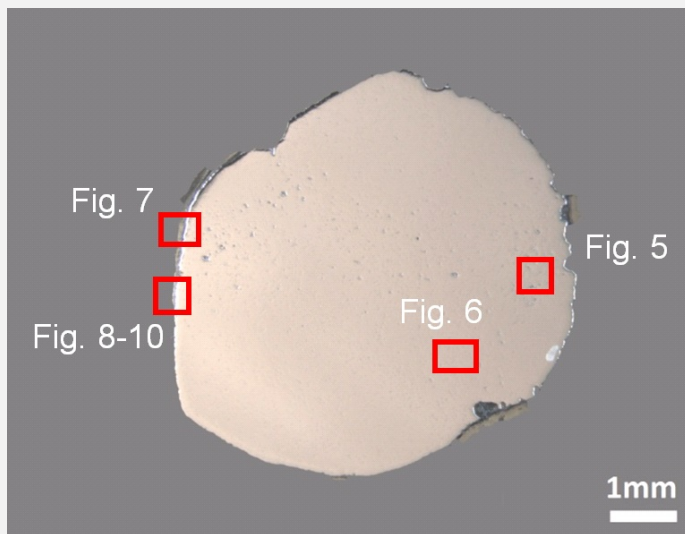
Fig. 2: Location of sampling area,

Binocular observation and representation of the corrosion structure

Stratigraphic representation: none.

MiCorr stratigraphy(ies) – Bi

Sample(s)



Credit HE-Arc CR.

Fig. 3: Micrograph of the cross-section showing the location of Figs. 5 to 10,

<b>Description of sample</b>	This cross-section shows a lateral cut through the tang (Fig. 2). Most of the corrosion crust is absent (Fig. 3).
<b>Alloy</b>	Leaded Bronze
<b>Technology</b>	Cold worked after annealing
<b>Lab number of sample</b>	MAH 87-196
<b>Sample location</b>	Musées d'art et d'histoire, Genève, Geneva
<b>Responsible institution</b>	Musées d'art et d'histoire, Genève, Geneva
<b>Date and aim of sampling</b>	1987, metallography and corrosion characterisation

## Complementary information

Nothing to report.

## Analyses and results

### Analyses performed:

Metallography (etched with ferric chloride reagent), Vickers hardness testing, ICP-OES, SEM/EDS, XRD.

## Non invasive analysis

## Metal

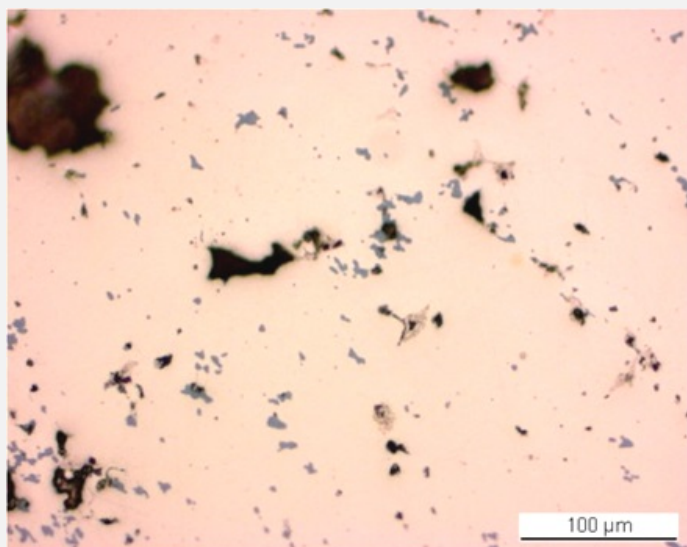
The remaining metal is a leaded bronze (Table 1) containing numerous copper sulphide and tiny Pb inclusions (Figs. 5-7, 10 and Table 2). The porosity within the metal is high, particularly along a band through the middle of the sample (Figs. 3 and 5). The etched structure of the leaded bronze shows small, regular polygonal grains, some with twinning (Fig. 6). Strain lines appear in grains close to the metal surface (Fig. 7). The average hardness of the metal is HV1 120.

Elements	Cu	Sn	Pb	Ni	Sb	As	Co	Ag	Fe	Zn
mass%	87.52	8.02	1.46	1.04	0.81	0.60	0.24	0.21	0.05	0.03

Table 1: Chemical composition of the metal. Method of analysis: ICP-OES, Laboratory of Analytical Chemistry, Empa.

Elements	O	S	Fe	Cu	Total
mass%	1.5	20	1.0	71	93

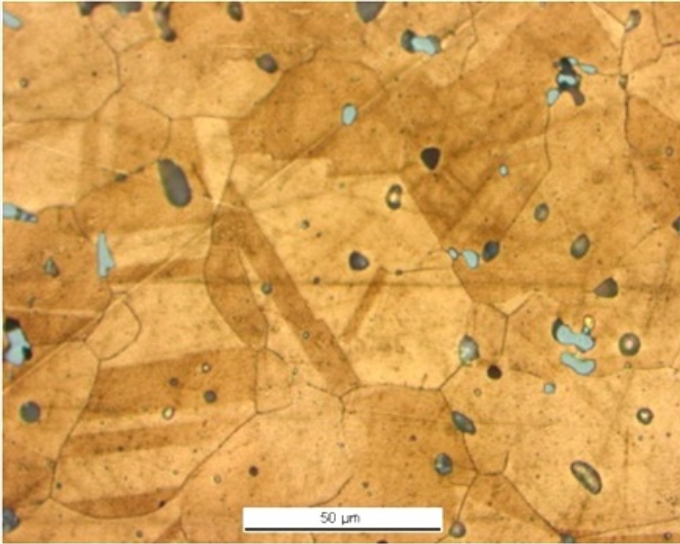
Table 2: Chemical composition of dark-grey inclusions. Method of analysis: SEM/EDS, Laboratory of Analytical Chemistry, Empa.



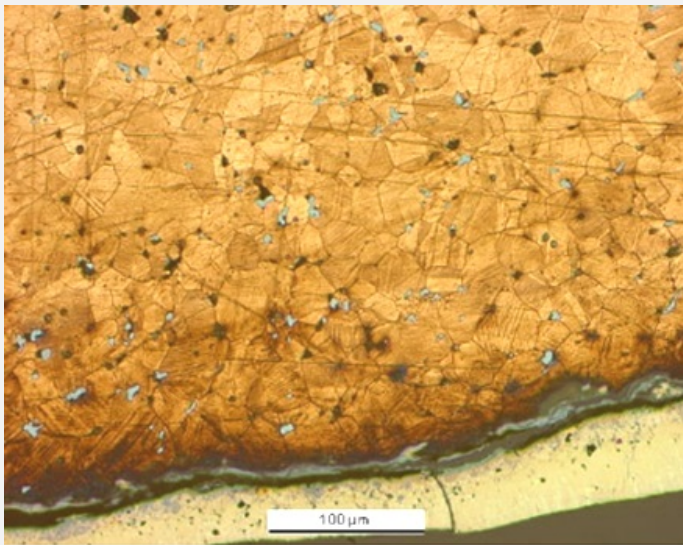
Credit HE-Arc CR.

Fig. 5: Micrograph of the metal sample from Fig. 3 (detail), unetched, bright field. In pink the metal, in black the porosity and in dark-grey copper sulphide inclusions,

Fig. 6: Micrograph of the metal sample from Fig. 3 (detail), etched, bright field. Angular and twinned grains are revealed as well as copper sulphide inclusions in grey,



Credit HE-Arc CR.



Credit HE-Arc CR.

Fig. 7: Micrograph of the metal sample from Fig. 3, etched, bright field (rotated by 270°, detail). Angular grains with strain lines can be seen as well as copper sulphide inclusions in grey,

<b>Microstructure</b>	Polygonal and twinned grains + strain lines (metal surface) with pores
<b>First metal element</b>	Cu
<b>Other metal elements</b>	Ni, Sn, Pb

**Complementary information**

Nothing to report.

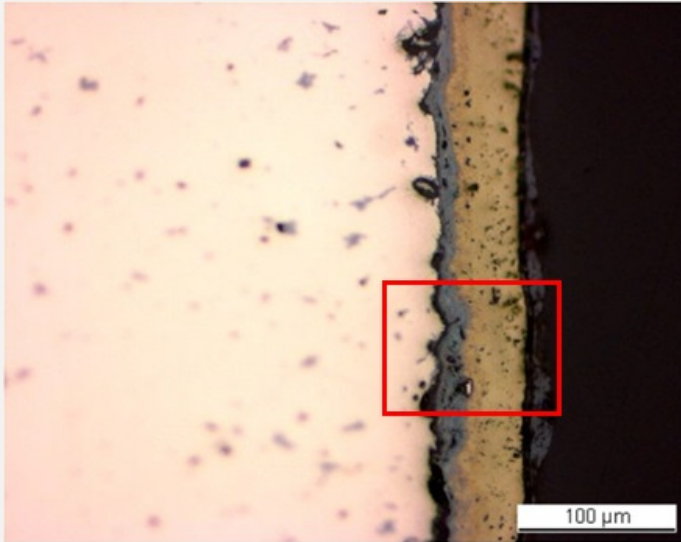
⌵ Corrosion layers

The metal has lost most of its original corrosion crust, the remainder having an average thickness between 60 and 190µm (Fig. 3). In some areas up to three corrosion layers are visible (Fig. 8). In polarised light (Fig. 9), the corrosion stratigraphy appears more clearly: it is composed of a dense black inner layer, an intermediate thick brown layer with bright spots (indicating porosity) and an outer red layer with white particles. The elemental chemical distribution of the SEM image reveals that the black inner layer (CP3) is Sn-rich, but contains Cu, O, Fe, Si, P, Pb, Ni, As, Ca and S (Table 3, Fig. 10). The brown layer (CP2) contains S, Fe and Cu and has a composition similar to chalcopyrite/CuFeS<sub>2</sub> (Table 3, Fig. 10). This was confirmed by past XRD analyses carried out by Schweizer (1994, museum report (1987)). The red layer (CP1) is an iron oxide (main elements Fe and O) and is contaminated with calcite/CaCO<sub>3</sub> particles (Table 3, Fig. 10).

Elements	O	Fe	Ni	Cu	Si	P	S	Ca	As	Sn	Pb	Total

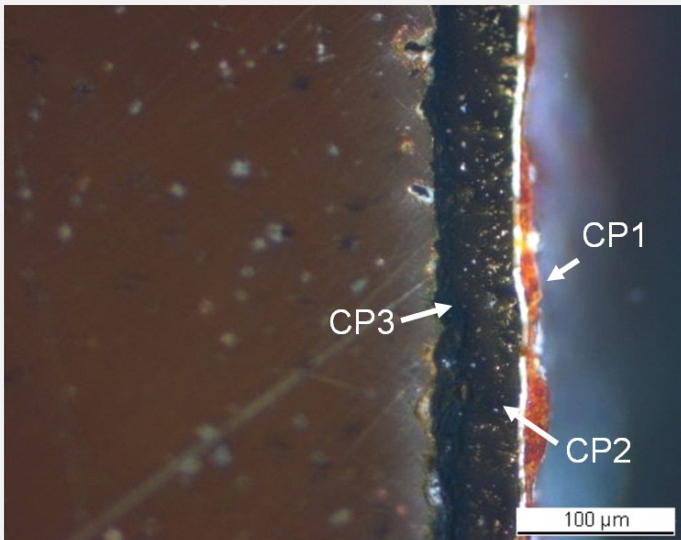
CP1, red layer	37	51	1.8	<	<	<	<	1.5	0.8	<	<	93
CP2, brown layer	<	30	<	42	<	<	35	<	<	<	<	107
CP2, white particles	50	<	<	0.6	<	<	<	39	<	<	<	90
CP3, black layer	39	4.8	1.2	5.2	3.9	3.7	<	<	0.7	37	3.7	100

Table 3: Chemical composition (mass %) of the corrosion layers (from Figs. 8 and 9). Method of analysis: SEM/EDS, Laboratory of Analytical Chemistry, Empa.



Credit HE-Arc CR.

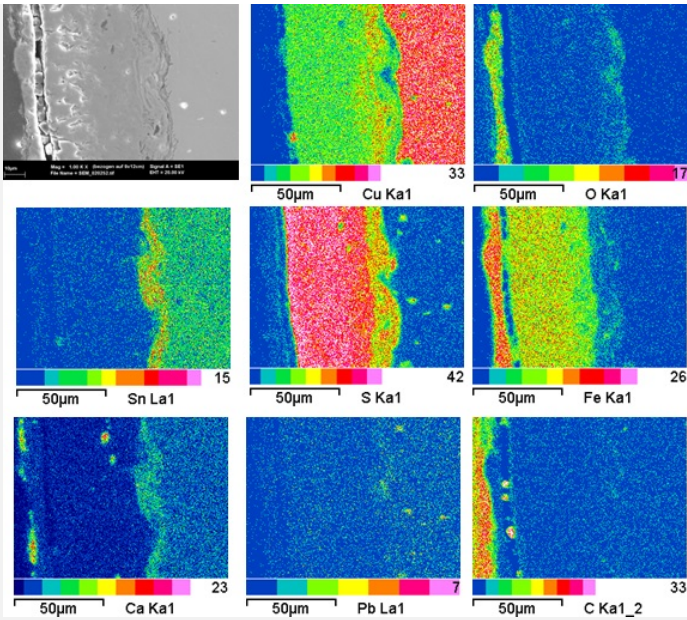
Fig. 8: Micrograph of the metal sample from Fig. 3 (reversed picture, detail), unetched, bright field. From left to right: metal (in pink), inner light-grey layer, intermediate brown layer and top dark-grey layer. The mapped area of Fig. 10 is marked by a square,



Credit HE-Arc CR.

Fig. 9: Micrograph of the same area as Fig. 8 and corresponding to the stratigraphy of Fig. 4, polarized light. From left to right: metal (in brown) covered with a corrosion crust consisting of a black layer, an intermediate brown layer with bright spots, a crack (white line) and a red layer with white particles,

Fig. 10: SEM image, SE-mode, and elemental chemical distribution of the selected area of Fig. 7 (reversed picture). Method of examination: SEM/EDS, Laboratory of Analytical Chemistry, Empa,



Credit Empa.

**Corrosion form** Uniform - pitting  
**Corrosion type** Type I (Robbiola)

**Complementary information**

Nothing to report.

✧ MiCorr stratigraphy(ies) – CS

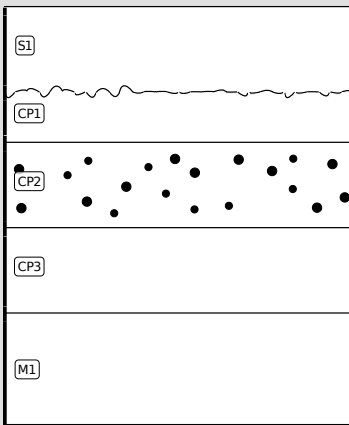


Fig. 4: Stratigraphic representation of the object in cross-section using the MiCorr application. This representation can be compared to Fig. 9, Credit HE-Arc CR.

✧ Synthesis of the binocular / cross-section examination of the corrosion structure

Corrected stratigraphic representation: none.

✧ Conclusion

The tang fragment is made from a leaded bronze and has been cold worked on the top surface after annealing. The SEM/EDS examination and past XRD analyses indicate the presence of chalcopyrite in the corrosion crust, typical of lake context (Schweizer 1994), enriched with Sn close to the metal surface and depleted of Cu on the outer surface. This object was certainly abandoned rather quickly in an anaerobic, humid and S and Fe-rich environment, favouring then the formation of chalcopyrite. The limit of the original surface most probably lies between the Sn-rich inner layer and the Fe and S-rich outer layers. The presence of iron oxides on top of the copper corrosion crust has not yet been explained. The corrosion is a type 1 according Robbiola et al. 1998.

## References

### *References on object and sample*

#### **References object**

1. Rychner-Faraggi A-M. (1993) Hauterive – Champréveyres 9. Métal et parure au Bronze final. Archéologie neuchâteloise, 17 (Neuchâtel).

#### **References sample**

2. Rapport d'examen, Laboratoire Musées d'art et d'histoire, Geneva GE (1987), 87-194 à 197

3. Schweizer, F. (1994) Objets en bronze provenant de sites lacustre: de leur patine à leur biographie. In: L'œuvre d'art sous le regard des sciences (éd. Rinuy, A. and Schweizer, F.), 143-157.

### *References on analytic methods and interpretation*

4. Robbiola, L., Blengino, J-M., Fiaud, C. (1998) Morphology and mechanisms of formation of natural patinas on archaeological Cu-Sn alloys, Corrosion Science, 40, 12, 2083-2111.